Excitation and polarization effects in semiconductor four-wave-mixing spectroscopy

Y. Z. Hu, R. Binder, and S. W. Koch*
Optical Sciences Center, University of Arizona, Tucson, Arizona 85721

S. T. Cundiff,* H. Wang,† and D. G. Steel
H. M. Randall Laboratory of Physics, University of Michigan, Ann Arbor, Michigan 48109
(Received 24 November 1993; revised manuscript received 28 February 1994)

The dependence of optical four-wave-mixing (FWM) signals in semiconductors on carrier density and laser-field polarization is investigated. The theoretical and experimental analysis reveals the importance of the excitation-induced dephasing processes for the understanding of numerous published results on polarization selections rules in FWM signals. Even apparently contradictory earlier findings can be explained with this theoretical model.

I. INTRODUCTION

During the last few years, a variety of investigations have been performed to study carrier spin-flipping processes in semiconductors and quantum wells. In addition to theoretical analysis,[1–3] experiments have investigated photoluminescence,[4] spectral-hole-burning[5,6] pump-probe,[7] four-wave-mixing (FWM), and photon-echo[8–14] phenomena. In these experiments, polarized laser pulses are used to excite and distinguish different spin states of the interband transitions, which, in GaAs, are the heavy-hole (hh) and light-hole (lh) excitons. Most theoretical investigations of ultrafast FWM phenomena are based on the semiconductor Bloch equations (SBE),[15,16] which have been used to explain successfully the observed temporal evolution of transient FWM signals in semiconductors as a consequence of coherent many-body exchange effects.[16,12] Solutions of the multiband semiconductor Bloch equations, which include valence-band effects described by the Luttinger Hamiltonian, show that in the low-excitation regime two opposite circularly polarized fields do not induce a FWM signal.[17] This has also been observed experimentally.[14,18] For other pump-probe polarization vectors, however, theoretical explanations of the experimental findings are less successful,[12,18,19] and even contain apparent contradictions. For example, the FWM signal $I_{\parallel}$ from two linearly copolarized pulses differs from $I_{\perp}$, the signal from linearly cross-polarized pulses, by an order of magnitude, under otherwise the same experimental conditions.[18] These observations are in contradiction to theoretical predictions based on perturbational calculations[19] or numerical integration of the SBE. Both approaches lead to the same conclusion that $I_{\parallel}$ and $I_{\perp}$ would have the same FWM signal intensity, and the signal would be linearly polarized in the probe field direction. Furthermore, recent experimental studies show that the polarization and intensity of the generated FWM signal exhibit complicated carrier-density dependences in both strained semiconductors and semiconductor quantum wells.[18,20]

In this paper, we present a theoretical analysis of the polarization dependence of FWM signals based on the SBE. For clarity, we restrict ourselves to GaAs systems with large hh-lh splitting. We take into account possible doping or preexcitation effects by means of a carrier-density-dependent dephasing rate. Also, the pump-induced density change and the resulting change in the dephasing rate are included. These excitation-induced dephasing (EID) processes have recently been found to be crucial in the understanding of FWM signals in a preexcited sample, in which they can give detailed information about microscopic dephasing processes.[20] This paper is organized as follows. In Sec. II the multiband semiconductor Bloch equations and the EID effect are briefly discussed. In Sec. III we perform third-order perturbation calculations to obtain FWM polarization selection rules. In Sec. IV, the numerical solutions of the multiband semiconductor Bloch equations are presented. The solutions verify the FWM polarization selection rules, and show that energetic inhomogeneity may cause different dephasing times in $I_{\parallel}$ and $I_{\perp}$ measurements.

II. BASIC MODEL

Within the screened Hartree-Fock approximation, the wave-vector-dependent optical polarization $P_{sj}(\mathbf{k})$ for the transition between the conduction band with spin s and the valence band with angular momentum quantum number j is governed by the polarization equation of the SBE ($\hbar=1$ throughout this paper)

$$i\frac{\partial P_{sj}(\mathbf{k})}{\partial t}=[-i\gamma_{sj}(N)+\mathcal{E}_k]P_{sj}(\mathbf{k})+\sum_{j'}\mathcal{T}_{jj'}(\mathbf{k})P_{sj'}(\mathbf{k}) -[1-n_s(\mathbf{k})]\Omega_{sj}(\mathbf{k})+\sum_{j'}N_{jj'}(\mathbf{k})\Omega_{sj'}(\mathbf{k}) , \quad (1)$$

and the corresponding hole and electron density equations are

$$\frac{\partial N_{jj'}(\mathbf{k})}{\partial t}=-i\sum_{j''}[\mathcal{T}_{j'j''}(\mathbf{k})N_{jj''}(\mathbf{k})-\mathcal{T}_{j''j}(k)N_{j''j'}(\mathbf{k})] +i\sum_{s}[\Omega_{sj'}(\mathbf{k})P^{*}_{sj}(\mathbf{k})-\Omega^{*}_{sj}(\mathbf{k})P_{sj'}(\mathbf{k})] , \quad (2)$$

$$\frac{\partial n_s(\mathbf{k})}{\partial t}=i\sum_j[\Omega_{sj}(\mathbf{k})P^*_{sj}(\mathbf{k})-\Omega^*_{sj}(\mathbf{k})P_{sj}(\mathbf{k})]\ , \tag{3}$$

where $\mathcal{E}_k$, $\mathcal{T}_{jj'}$, and $\Omega_{sj}(\mathbf{k})$ are the renormalized electron kinetic energy, Luttinger matrix elements, and Rabi energy, respectively.[17]

$$\Omega_{sj}(\mathbf{k})=\boldsymbol{\mu}_{sj}\cdot\mathbf{E}+\sum_{\mathbf{q}}V^s_{\mathbf{q}}P_{sj}(\mathbf{k}+\mathbf{q})\ ,$$

$$\mathcal{E}_{\mathbf{k}}=\varepsilon_{\mathbf{k}}-\sum_{\mathbf{q}}V^s_{\mathbf{q}}n_{\mathbf{k}+\mathbf{q}s}-\Sigma^{\mathrm{CH}}\ ,$$

$$\mathcal{T}_{jj'}(\mathbf{k})=T_{jj'}(\mathbf{k})-\sum_{\mathbf{q}}V^s_{\mathbf{q}}N_{\mathbf{k}+\mathbf{q}jj'}\ ,$$

$$\varepsilon_{\mathbf{k}}=E_g+\frac{k^2}{2m_e}\ ,$$

and

$$\Sigma^{\mathrm{CH}}=\sum_{j\mathbf{k}}[V^s(\mathbf{k})-V(\mathbf{k})]\ .$$

Here $\mathbf{E}$ is the external laser field and the dot product $\boldsymbol{\mu}_{sj}\cdot\mathbf{E}$ between the field vector and optical dipole moment $\boldsymbol{\mu}$ essentially determines the polarization selection rules. V and V^s are the unscreened and screened Coulomb potentials, respectively. E_g is the band-gap energy. m_e is the electron effective mass. We use the Luttinger Hamiltonian to describe the more complicated valence-band structure. $T_{jj'}(\mathbf{k})$ are the usual 4×4 Luttinger Hamiltonian matrix elements. Equations (1)–(3) have the same form as the multilevel optical Bloch equations; however, the many-body exchange effects strongly modify physical parameters such as the effective electric field and semiconductor band structure. In Eq. (2), terms proportional to $N_{jj''}N_{j''j'}$ are neglected.

In the case of large hh-lh splitting it is sufficient to investigate only the two hh transitions with $(s,j)=\{(-\frac{1}{2},\frac{3}{2}),(+\frac{1}{2},-\frac{3}{2})\}$.[17] Within the screened Hartree-Fock approximation, the imaginary part of the Coulomb hole and exchange self-energy introduces an effective dephasing term in the semiconductor Bloch equations.[20] Equation (1) generalizes the corresponding Hartree-Fock equations derived in Ref. 17 in an important way: the dephasing rate depends explicitly on the carrier density. This accounts for carrier-carrier scattering, which is not included in the Hartree-Fock scheme. A possible theoretical approach to the unified description of optical properties and incoherent carrier scattering processes is the nonequilibrium Green's-function technique.[21,22] Generally, the optical polarization appears as a one-particle Green's function. The equation of motion for this function contains various contributions, all of which can be written as the products of a self-energy times a Green's function. In the simplest case of the Hartree-Fock self-energy, the equation reduces to the one in Ref. 17, where all Coulomb contributions stem from self-energy terms. In more involved approximation schemes, the self-energy depends on both the carrier distribution and optical polarization functions. The complex self-energy determines, for example, the renormalization of the one-particle energies (the real part of the self-energy) and the level broadening describing damping of the states (imaginary part of the self-energy). The choice of the approximation scheme that determines the concrete form of the self-energy depends on the physical situation. For example, an electron-hole plasma can be well described within the screened Hartree-Fock (SHF) approximation. To treat an exciton gas or an exciton-plasma mixture, one should consider an approximation beyond the SHF (see Ref. 21 and the contribution of Schäfer in Ref. 22). However, a self-consistent treatment of the screening properties of an exciton gas or exciton-plasma mixture within the semiconductor Bloch equations is presently far beyond our numerical capabilities. Whereas such a microscopic theory will certainly undergo a long future investigation, we can already draw important conclusions from the mere fact that the dephasing rate is in principle density dependent. Moreover, we can use very simple microscopic models for an approximate treatment of this density dependence. The simplest approach, used in Ref. 20, is to assume that the dephasing can be treated within a quasithermal equilibrium limit of the SHF. The dephasing rate is given in Ref. 22 as Eq. (4.66). For a concrete evaluation of these equations we need a model for the longitudinal screening function. An excitonic plasmon pole screening function [similar to Eqs. (5.102)-(5.104) in Ref. 22)] contains valuable information.

Sufficiently weak pump pulses allow the linearization of the excitation-induced dephasing rate $\gamma_{sj}(N)$ around the density N_0:

$$\gamma_{sj}(N)\simeq\gamma_0+\left.\frac{\partial\gamma_{sj}}{\partial N}\right|_{N_0}\Delta N\ . \tag{4}$$

Here $\gamma_0=\gamma_{sj}(N_0)$, and ΔN is the carrier density excited by the pump and probe fields. Typical dephasing saturation is reflected in an increase of the effective dephasing rate and a decrease of the EID term $\partial\gamma_{sj}/\partial N$ with increasing N. The fact that EID contains the total density, $\Delta N=\sum N_a$ with $a=\{j,s\}$, yields a strong coupling of the two hh transitions, which correspond to the two angular momentum eigenstates $J_z=\pm1$. We denote these transitions as σ_+ and σ_- transitions, respectively.

III. PERTURBATIONAL APPROACH

Qualitatively, the FWM polarization selection rules are not affected by the presence of the coherent exchange effects. Neglecting these exchange effects makes analytical solutions of Eq. (1) possible for stationary (cw) fields or ultrashort pulses. If only the heavy-hole bands are taken into account, the simplified polarization equation is

$$\begin{aligned}i\frac{\partial P_{sj}(\mathbf{k})}{\partial t}=&-i\left[\gamma_0+\left.\frac{\partial\gamma_{sj}}{\partial N}\right|_{N_0}\Delta N\right]P_{sj}(\mathbf{k})\\&+\left[E_kP_{sj}(\mathbf{k})-\sum_{\mathbf{q}}V^s_{\mathbf{q}}P_{sj}(\mathbf{k}+\mathbf{q})\right]\\&-(\boldsymbol{\mu}_{sj}\cdot\mathbf{E})[1-2f_{sj}(\mathbf{k})]\ ,\end{aligned} \tag{5}$$

where the Luttinger Hamiltonian is replaced by an effective heavy-hole Hamiltonian, i.e., $E_k=(1/2m_e+1/2m_h)k^2+E_g$. In Eq. (5) we denote

$f_{sj}(\mathbf{k})=n_s(\mathbf{k})=N_{jj'}(\mathbf{k})\delta_{jj'}$. Furthermore, Eq. (5) can be transformed into the polarization equation of the two-level system by expanding $P_{sj}(\mathbf{k})$ and $f_{sj}(\mathbf{k})$ in terms of the exciton wave functions and keeping only the ground-state wave function in the equation. This way we obtain the optical Bloch equations of the two-level system:

$$i\frac{\partial P_{sj}}{\partial t}=\left[\omega_0-i\left[\gamma_0+\delta_{sj}\sum_{s'j'}F_{s'j'}\right]\right]P_{sj}$$
$$-(\boldsymbol{\mu}_{sj}\cdot\mathbf{E})[|\varphi^*(r=0)|^2-2F_{sj}]\ , \tag{6}$$

where $\omega_0=E_g-E_R$ with the exciton Rydberg energy E_R, P_{sj} and $F_{sj}=\sum_{\mathbf{k}}f_{sj}(\mathbf{k})$ are the total polarization and carrier density, respectively, $\varphi(r)$ is the ground-state eigenfunction of the Wannier equation, and

$$\delta_{sj}=\left.\frac{\partial\gamma_{sj}}{\partial F}\right|_{f_0}\ .$$

In the same manner, the density equation (2) can be simplified into the population equation of the two-level Bloch equations.

In general, a polarized incident laser field is given by $\mathbf{E}=\sum_i E_i(\alpha_i\boldsymbol{\sigma}_+ +\beta_i\boldsymbol{\sigma}_-)$, where $\boldsymbol{\sigma}_+$ and $\boldsymbol{\sigma}_-$ are the unit circular field polarization vectors with angular momentum $+1$ and -1, respectively. The summation index i counts all the different incident light beams, e.g., $i=1,2$ in a standard two-pulse FWM setup, denoting the probe and pump field, respectively. In a typical two-beam self-diffracted FWM setup, the stronger beam (pulse 2) propagates along the direction $\mathbf{K}_2$, the weaker beam (pulse 1) is in the direction $\mathbf{K}_1$ and the induced FWM signal travels along $2\mathbf{K}_2-\mathbf{K}_1$. For the cw degenerate field-induced FWM signal, the optical Bloch equations can be solved perturbatively up to the third order. If we denote the outgoing signal as $\mathbf{E}_{\rm FWM}=E_+\boldsymbol{\sigma}_+ +E_-\boldsymbol{\sigma}_-$, we find

$$E_+\propto 2\alpha_2\alpha_2\alpha_1^*+\frac{\delta}{(\gamma_0+i\Delta)}(\alpha_2\alpha_2\alpha_1^*+\alpha_2\beta_2\beta_1^*)\ , \tag{7}$$

$$E_-\propto 2\beta_2\beta_2\beta_1^*+\frac{\delta}{(\gamma_0+i\Delta)}(\beta_2\beta_2\beta_1^*+\beta_2\alpha_2\alpha_1^*)\ . \tag{8}$$

Here, $\Delta=\omega-\omega_0$ is the detuning of the pump fields with respect to the exciton resonance energy.

The polarization selection rules of the two-beam FWM experiments corresponding to Eqs. (7) and (8) are given in Table I. Different polarization combinations of $\mathbf{E}_2$ and $\mathbf{E}_1$ are listed in the first two columns, and the corresponding polarization vector of the induced FWM signal is given in the last two columns. Zeros indicate forbidden transitions. Two sets of polarization selection rules appear in different parameter regimes. For $\delta\ll\gamma_0$, which corresponds to the high-carrier-density limit,[20] $I_\parallel$ and $I_\perp$ have similar signal magnitudes. The same result is obtained using the equation for noninteracting two-level systems.[19] In contrast, $I_\perp$ is much smaller than $I_\parallel$ if $\delta\gg\gamma_0$, which is appropriate for relatively low carrier densities. In addition to the usual FWM scattering mechanism (scattering of the pump field and pump-induced polarization at its own density grating[16]) in Eq. (1), EID introduces a channel through which the σ_+ polarization can be scattered by the σ_- density grating, and vice versa. If $\mathbf{E}_1\|\mathbf{E}_2$, all three mechanisms contribute to FWM signals. However, for $\mathbf{E}_1\perp\mathbf{E}_2$ the contribution due to EID is canceled because the σ_+ density grating differs from the σ_- grating by a phase factor of π. Therefore, only the first two scattering mechanisms contribute to the FWM signal. By changing the relative polarization of the pump and probe, we can modify the magnitude of the EID-induced FWM signals from the maximum at $\mathbf{E}_2\|\mathbf{E}_1$ to its minimum at $\mathbf{E}_2\perp\mathbf{E}_1$. If EID is the dominant scattering contribution, then $I_\parallel\gg I_\perp$, while $I_\parallel\simeq I_\perp$ if EID is insignificant.

TABLE I. Polarization selection rules of two-beam FWM.

Excitation		Signal	
Pump	Probe	$\delta\ll\gamma_0$	$\delta\gg\gamma_0$
X	X	X	X
X	Y	Y	0[a]
σ_+	σ_+	σ_+	σ_+
σ_+	σ_-	0	0
σ_+	X	σ_+	σ_+
X	σ_+	σ_+	X

[a]Here the FWM signal is not exactly zero, but small compared with $I_\parallel$. It is also Y polarized.

If both pump and probe fields are linearly polarized with a relative angle θ, the FWM signal is also linearly polarized. The dependence of the signal intensity on the incident polarization angle is found to be

$$I(\theta)\propto \sin^2(\theta)+(1+\delta/\gamma_0)^2\cos^2(\theta)\ , \tag{9}$$

and the polarization of the FWM signal is

$$\theta_{\rm FWM}=-\tan^{-1}\left[\frac{\tan(\theta)}{1+\delta/\gamma_0}\right]\ . \tag{10}$$

In a recent experiment,[18] $\theta_{\rm FWM}$ and $I(\theta)$ have been measured in a 27-nm-wide GaAs quantum well. Those results show a very similar θ dependence as that predicted by Eqs. (9) and (10), if the small carrier density in Ref. 18 corresponds to $\delta\gg\gamma_0$, and the high density corresponds to $\delta\ll\gamma_0$.

We now extend the perturbation calculation to the three-beam backward FWM configuration. In this setup, one uses two counterpropagating pump beams ($\mathbf{E}_2$ and $\mathbf{E}_3$) and a probe field ($\mathbf{E}_1$) which propagates at a small angle with respect to the pump pulses. A FWM signal, propagating along the direction $-\mathbf{K}_1$, is created from the scattering of one of the pump pulses by the density grating due to the probe and the other pump pulse. For the FWM signal, we find

$$E_+\propto 4\alpha_1^*\alpha_2\alpha_3+\frac{\delta}{(\gamma_0+i\Delta)}[2\alpha_1^*\alpha_2\alpha_3+\beta_1^*(\alpha_2\beta_3+\alpha_3\beta_2)]\ , \tag{11}$$

$$E_-\propto 4\beta_1^*\beta_2\beta_3+\frac{\delta}{(\gamma_0+i\Delta)}[2\beta_1^*\beta_2\beta_3+\alpha_1^*(\beta_2\alpha_3+\beta_3\alpha_2)]\ . \tag{12}$$

The corresponding three-beam FWM polarization selection rules are listed in Table II. When EID is the dominant scattering mechanism, a FWM signal is allowed as long as the circular polarization of the probe is identical to one of the two pump fields. In the opposite limit (no EID) a FWM signal occurs only if all three beams have the same circular polarization.

Our experimental three-beam FWM results are also summarized in Table II. The measurements are taken on a 100-Å GaAs multiple-quantum-well sample which is described in Ref. 11. The three pulses have 3 ps autocorrelation widths and a fixed delay of 5 ps. The carrier density is less than 1×10^{8} cm^{-2}. Table II lists the observed relative FWM intensities for various pump and probe polarizations. Note that in Table II only the theoretical possibilities of signals with certain polarizations are given, whereas the relative signal strengths are omitted. For $\delta\gg\gamma_0$, Eqs. (11) and (12) show that the FWM strength induced by $\sigma_+\sigma_-\sigma_+$ pulses is one half of that induced by $\sigma_+\sigma_+\sigma_+$. In our experiment this ratio is between $\frac{1}{3}$ and $\frac{1}{4}$. This observation indicates that EID is the dominant contribution for our experimental conditions. The experimental results presented in Table II exhibit very weak nonzero signals for polarizations, for which theoretically no signal is expected. These signals are on the order of that expected due to residual ellipticity arising from birefringence in the optical elements, and hence are not considered significant.

We also measured the degree of polarization, defined by $p=(I_+-I_-)/(I_++I_-)$, where $I_+(I_-)$ is the $\sigma_+(\sigma_-)$ component of the FWM intensity, as a function of the pump-excited carrier density for various field polarization vectors. In Fig. 1 we show results for the case where the first and second pulses are cocircularly polarized and the third is linearly polarized. At low intensities, where a $\chi^{(3)}$ analysis is justified, the results agree with the predictions of Eqs. (11) and (12) that the signal is linearly polarized along the direction of the third pulse. At high intensities, the FWM signal is nearly circularly polarized in the same sense as the first and second pulses. Although this behavior requires a treatment beyond $\chi^{(3)}$, it can intuitively be understood on the basis of Eqs. (11) and (12). In this case, pump-excited carriers contribute similarly to $\partial\gamma_{sj}/\partial N$ as the preinjected carriers, resulting in a reduced EID parameter, δ. If $\delta\ll\gamma_0$, Eqs. (11) and (12) show that $p=1$.

IV. NUMERICAL SOLUTIONS

To compute transient two-beam FWM signals, including many-body exchange and EID effects, we solve numerically the multiband semiconductor Bloch equations. Details of such an analysis without EID are given in Ref. 17. The EID parameter $\partial\gamma_{sj}/\partial N$ is estimated using the excitonic "plasmon pole" approximation.[20,21] In addition to the FWM, we account for the preexcitation by a prepulse, which is at least one order of magnitude stronger than the pump field. The numerical solution of the SBE essentially confirms the results of Table I. The exchange effects, however, enhance the dependence of $I_{\parallel}/I_{\perp}$ on the EID parameter by about an order of magnitude. The time-integrated self-diffracted FWM signal as a function of θ, induced by two linearly polarized fields, is plotted in Fig. 2. The low density results show an almost vanishing FWM signal for linearly cross-polarized pulses, because in this case the dominant light-scattering mechanism is EID. A weaker polarization dependence of the

TABLE II. Polarization selection rules of three beam FWM.

Excitation			Theory		Experiment	
E_1	E_2	E_3	$\delta\ll\gamma_0$	$\delta\gg\gamma_0$	σ_+	σ_-
σ_+	σ_+	σ_+	σ_+	σ_+	299.0	7.5
σ_-	σ_+	σ_+	0	0	5.4	0.38
σ_+	σ_-	σ_+	0	σ_-	3.8	96.6
σ_+	σ_+	σ_-	0	σ_-	2.3	66.0

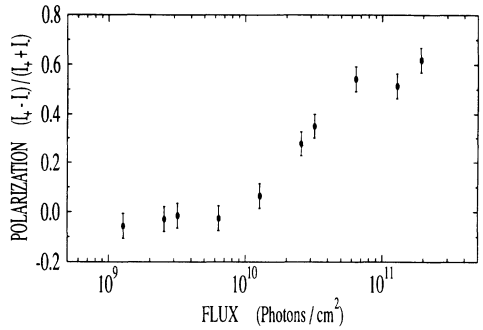

FIG. 1. Polarization of the emitted signal for the circularly copolarized first and second pulses and linearly polarized third pulse. A value of +1 indicates cocircular polarization with respect to the first two fields, and zero corresponds to linear polarization.

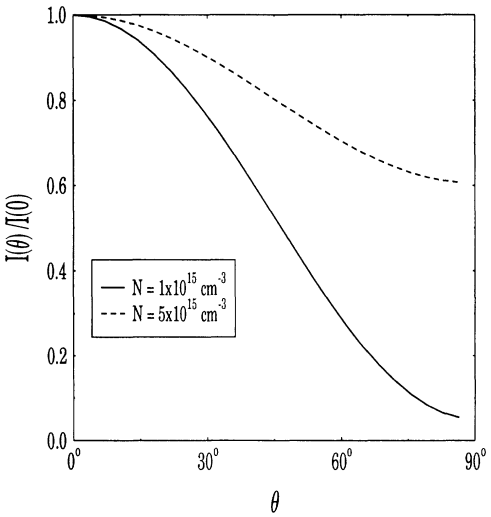

FIG. 2. Time-integrated FWM signal from the heavy-hole exciton at $T=20$ K vs the relative angle between the two incident polarization vectors. Delay time is 300 fs and $T_2=100$ fs. The preexcited carrier density is $N_0=1\times10^{15}$ (solid line) and 5×10^{15} cm^{-3} (dashed line), respectively. The field strengths are $\mu_{cv}E_2=0.01E_R$ and $\mu_{cv}E_1=0.001E_R$ at the respective pulse maximum (μ_{cv} is the dipole matrix element).

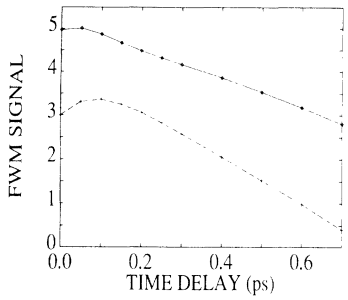

FIG. 3. Time-integrated FWM signal (in arb. units) of an inhomogeneous system as a function of time delay for linearly copolarized (solid line) and cross-polarized (dashed line) pulses. $N_0 = 10^{15}$ cm^{-3}. The inhomogeneous broadening is 1.9 meV. Other parameters are the same as in Fig. 2.

FWM signal is found for large densities, which, again, can be explained as a consequence of the decreasing EID contribution at higher densities. The results of Fig. 2 confirm the predictions of Eq. (9).

We now consider the effects of spatial inhomogeneity. In Refs. 11, 14, and 23 it was found that in quantum wells $I_\perp$ and $I_\parallel$ decay differently. This phenomenon was assigned to energy inhomogeneities and a disorder-induced breaking of the rotational symmetry.[24] Our numerical SBE solutions and perturbation calculations show that $I_\parallel$ and $I_\perp$ have identical dephasing times if the system is homogeneous. However, taking spatial inhomogeneities into account via a statistical Gaussian distribution of the band gap, we find that EID also leads to different dephasing times for $I_\perp$ and $I_\parallel$. Since EID processes are fundamentally different from the disorder induced coupling in Ref. 24, further investigation is needed to determine the relative strengths of these two effects as a function of the sample parameters. Figure 3 shows the EID effects in inhomogeneous systems. Underlying this figure is an inhomogeneously broadened exciton resonance with an inhomogeneous broadening of 1.9 meV. We clearly find different decay rates for $I_\perp$ and $I_\parallel$.

Finally, we want to mention another experimental result which supports the EID model. In Ref. 14 it is found that the difference between $I_\parallel$ and $I_\perp$ vanishes if an external magnetic field is applied. Here, the energetic degeneracy of the σ_+ and σ_- transition is lifted. As a consequence, the EID-induced FWM signal in $I_\perp$, which in the degenerate case vanishes due to a cancellation of the density grating from the two degenerate transitions, no longer vanishes.

In summary, our theoretical and experimental investigations show that excitation-induced dephasing contributes significantly to FWM signals. Previously unexplained FWM polarization selection rules can be explained using our EID model. These selection rules obtained from the third-order perturbation and numerical calculations agree with a recent $\chi^{(3)}$ analysis of full many-body equations.[25]

ACKNOWLEDGMENTS

We acknowledge financial support from NSF, ARO, AFOSR, NEDO, and OCC at the University of Arizona, and grants for CPU time at the Pittsburgh Supercomputer Center and the CCIT, University of Arizona.

*Present address: Fachbereich Physik und Wissenschaftliches Zentrum für Materialwissenschaften, Philipps-Universität, Mainzergasse 33, 35032 Marburg, Federal Republic of Germany.

†Present address: AT&T Bell Laboratories, Holmdel, NJ 07733.

[1] T. Uenoyama and L. J. Sham, Phys. Rev. B **42**, 7114 (1990); M. Z. Maialle, E. A. de Andrada e Silva, and L. J. Sham, *ibid.* **47**, 15 776 (1993).

[2] R. Ferreia and G. Bastard, Phys. Rev. B **43**, 9687 (1991).

[3] *Optical Orientation,* edited by F. Meier and B. Zakharchenya (North-Holland, Amsterdam, 1984).

[4] T. C. Damen, L. Vina, J. E. Cunningham, and L. J. Shah, Phys. Rev. Lett. **67**, 3432 (1991).

[5] H. Wang, M. Jiang, and D. G. Steel, Phys. Rev. Lett. **65**, 1255 (1991).

[6] H. Wang, M. Jiang, R. Merlin, and D. G. Steel, Phys. Rev. Lett. **69**, 804 (1992).

[7] S. Bar-Ad and I. Bar-Joseph, Phys. Rev. Lett. **64**, 349 (1992).

[8] L. Schultheis, J. Kuhl, A. Honold, and C. W. Tu, Phys. Rev. Lett. **57**, 1635 (1986).

[9] L. Schultheis, J. Kuhl, A. Honold, and C. W. Tu, Phys. Rev. Lett. **57**, 1797 (1986).

[10] K. Leo, E. Göbel, T. C. Damen, J. Shah, S. Schmitt-Rink, W. Schäfer, J. F. Müller, K. Köhler, and P. Ganser, Phys. Rev. B **44**, 5726 (1991).

[11] S. T. Cundiff, H. Wang, and D. G. Steel, Phys. Rev. B **46**, 7248 (1992).

[12] D. S. Kim, J. Shah, T. C. Damen, W. Schäfer, S. Schmitt-Rink, and K. Köhler, Phys. Rev. Lett. **69**, 2725 (1992).

[13] M. Koch, D. Weber, J. Feldmann, E. O. Göbel, T. Meier, A. Schulze, P. Thomas, S. Schmitt-Rink, and K. Ploog, Phys. Rev. B **47**, 1532 (1993).

[14] O. Carmel and I. Bar-Joseph, Phys. Rev. B **47**, 7606 (1993).

[15] M. Lindberg and S. W. Koch, Phys. Rev. B **38**, 3342 (1988).

[16] M. Lindberg, R. Binder, and S. W. Koch, Phys. Rev. A **45**, 1865 (1992).

[17] Y. Z. Hu, R. Binder, and S. W. Koch, Phys. Rev. B **47**, 15 679 (1993).

[18] R. Eccleston, J. Kuhl, D. Bennhardt, and P. Thomas, Solid State Commun. **86**, 93 (1993).

[19] S. Schmitt-Rink, D. Bennhardt, V. Heuckeroth, P. Thomas, P. Haring, G. Maidorn, H. Bakker, K. Leo, D.-S. Kim, J. Shah, and K. Köhler, Phys. Rev. B **46**, 10 460 (1992).

[20] H. Wang, K. Ferrio, D. G. Steel, Y. Z. Hu, R. Binder, and S. W. Koch, Phys. Rev. Lett. **71**, 1261 (1993).

[21] H. Haug and S. Schmitt-Rink, Prog. Quantum Electron. **9**, 3 (1984).

[22] *Optical Nonlinearities and Instabilities in Semiconductors,* edited by H. Haug (Academic, New York, 1988).

[23] H. H. Yaffe, Y. Prior, J. P. Harbison, and L. T. Florez, J. Opt. Soc. Am. B **10**, 578 (1993).

[24] D. Bennhardt, P. Thomas, R. Eccleston, E. J. Mayer, and J. Kuhl, Phys. Rev. B **47**, 13 485 (1993).

[25] M. Lindberg, R. Binder, Y. Z. Hu, and S. W. Koch (unpublished).